# X-ray and neutron imaging - Complementary techniques for materials science and engineering

**Article** *in* International Journal of Materials Research (formerly Zeitschrift fuer Metallkunde) · September 2010

Impact Factor: 0.64 · DOI: 10.3139/146.110382



**9 authors**, including:

John Banhart
Technische Universität Berlin
**469** PUBLICATIONS **8,458** CITATIONS
SEE PROFILE

Francisco García-Moreno
Helmholtz-Zentrum Berlin
**124** PUBLICATIONS **1,106** CITATIONS
SEE PROFILE

Ingo Manke
Helmholtz-Zentrum Berlin
**312** PUBLICATIONS **4,793** CITATIONS
SEE PROFILE

Wolfgang Treimer
Beuth Hochschule für Technik Berlin
**114** PUBLICATIONS **1,565** CITATIONS
SEE PROFILE

International Journal of
MATERIALS RESEARCH

Zeitschrift für METALLKUNDE

B Basic





John Banhart[a,b], András Borbély[c,d], Krzysztof Dzieciol[a,c], Francisco Garcia-Moreno[a], Ingo Manke[a], Nikolay Kardjilov[a], Anke Rita Kaysser-Pyzalla[a,e], Markus Strobl[a], Wolfgang Treimer[a,f]

[a] Helmholtz-Zentrum Berlin für Materialien und Energie GmbH, Berlin, Germany
[b] Technische Universität Berlin, Institute of Materials Science and Technology, Berlin, Germany
[c] Ecole des Mines de Saint Etienne, Saint Etienne, France
[d] Max-Planck-Institut für Eisenforschung GmbH, Düsseldorf, Germany
[e] Ruhr-Universität Bochum, Bochum, Germany
[f] Beuth-Hochschule, Berlin, Germany

# X-ray and neutron imaging – Complementary techniques for materials science and engineering

*Dedicated to Professor Dr. H.-P. Degischer on the occasion of his 65th birthday*

Using X-ray and neutron radiography and tomography, images of material and component inhomogeneities and their development with time can be obtained. Due to their non-destructiveness and non-invasive nature both methods give insight into the function of devices and their decay processes. Fundamentals of X-ray and neutron radiography and tomography are briefly outlined, examples for both techniques are given, their complementarities are highlighted and emerging techniques and frontiers are discussed.

**Keywords:** Radiography; Tomography; Neutron; X-ray; Complementarity

## 1. Introduction

Very shortly after the discovery of X-rays in 1895, Wilhelm Conrad Röntgen realised that this penetrating radiation could be used to image interior features of objects such as the hand of his colleague in Würzburg that he obtained using the rays he discovered and baptised "X-rays", see Fig. 1a. The images show that different materials give rise to different grey scales and that the presumably metallic ring absorbs the largest part of the radiation. Thus, not only medical investigations, but, also engineering applications are possible using radiography.

After Sir James Chadwick had discovered the neutron as an elementary particle in 1932, it was straightforward to try to image objects with these particles too. One of the first to succeed were scientists in Berlin, including H. Kallmann, E. Kuhn and O. Peter, who set up neutron radiation sources and imaging systems. The first neutron radiograph seems to have been published in 1944 (see Fig. 1b) by O. Peter who worked for the research centre of the German Mail. This history has been reviewed by C.-O. Fischer at the Hahn-Meitner Institute, Berlin, in 1992 [1].

Both X-ray and neutron radiography continuously developed in the years after their invention, driven by better sources, better detecting systems and new applications [2–8]. An important step was the transition from simple 2D radiography to 3D tomography in 1972 by G. N. Hounsfield – first for X-rays – based on mathematical ideas created much earlier [2]. The mathematical foundation requires some specific properties of the interaction between beam and sample that both X-rays and neutrons satisfy to a sufficient approximation. Therefore, both X-ray and neutron tomography are feasible. It

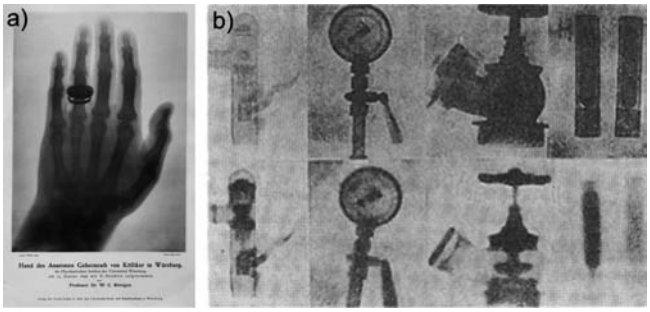


Fig. 1. Historical radiographic images. (a) X-ray image taken by Röntgen in Würzburg in the year 1904, (b) neutron images taken by O. Peter in Berlin in 1944 [1].

took longer to develop neutron tomography than its X-ray counterpart simply because the fluxes of neutron sources are lower and the available 2D detectors less effective. Still, in the proceedings of the 4th World Conference on Neutron Radiography [1], 10 papers deal with neutron tomography, quite a new method in 1992. It was in the 1990s that tomography was largely facilitated by new digital image acquisition systems – a prerequisite for fast and reliable 3D imaging.

Today, X-ray tomography based on either X-ray tubes or synchrotron X-ray sources on the one hand, and neutron tomography using neutrons from reactors or spallation sources on the other hand are standard techniques available at many laboratories worldwide, see a selection of facilities in Refs. [2, 9–16]. A fairly new idea is to combine X-ray and neutron imaging to couple different contrast generation mechanisms. Such complementary investigations have become attractive only in the past decade since the spatial resolution of neutron imaging has been improved sufficiently [17–21]. In this review a brief overview to such complementary measurements – with a focus on results of the Helmholtz Centre Berlin for Materials and Energy – is given.

## 2. Interaction between X-rays, neutrons and matter

Most imaging experiments can be described by Fig. 2 or a slight variation of it [2]. In the case depicted, a very thin pencil beam, intensity ($I_0$), penetrates a sample. A part of it is absorbed ($I_a$), a part transmitted in the original direction, a third part deflected, i. e. scattered *out* ($I_{s,out}$). The detector measures a reduced intensity $I_t = I_0 - I_a - I_{s,out}$. Usually $I_t/I_0$ is given which can be written as $1-(I_a + I_{s,out})/I_0$. In this sense, absorption and scattering produce the same attenuating effect and in a homogeneous medium of thickness $d$, the Beer–Lambert law $I_t/I_0 \approx e^{-\mu d}$ holds, where $\mu$ is the linear attenuation coefficient of the material.

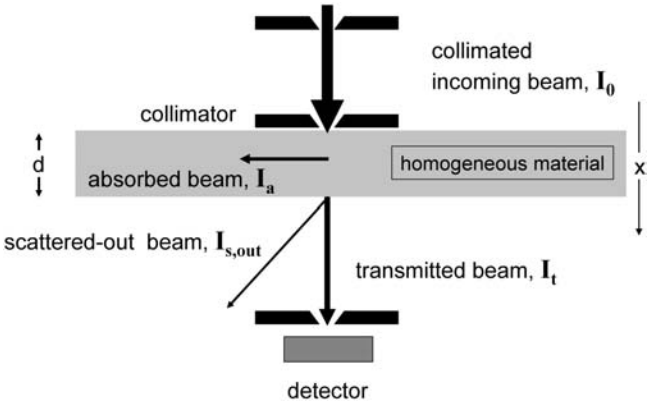


Fig. 2. Layout of an imaging experiment based on a pencil beam [5].

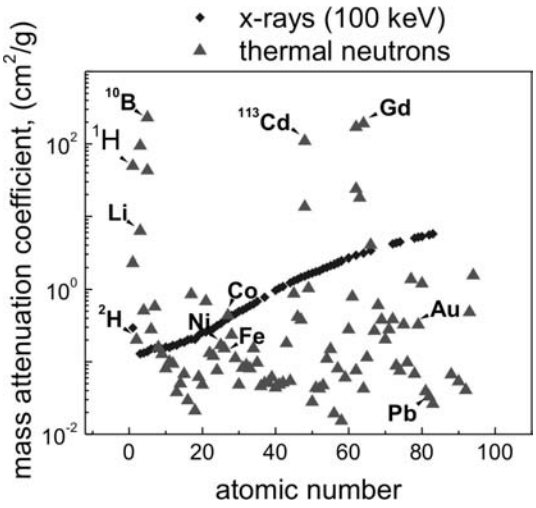


Fig. 3. Mass attenuation coefficient as a function of atomic number for all elements.

If a beam is used that extends over an area, the situation becomes more complicated. A detector position can now receive intensity scattered *in* from other parts of the beam, an effect that can only be treated in an approximate way [2].

For the simpler first case, Fig. 3 shows the mass specific attenuation coefficient $\mu_m$, i. e. $\mu$ over the density $\rho$ of the material is given as a function of the atomic number of the elements from $Z = 1$ (hydrogen) to $Z = 92$ (uranium).

The values shown as diamond symbols in Fig. 3 refer to X-rays of 100 keV energy. Obviously, $\mu_m$ varies in a smooth way with $Z$. This is because the interaction is governed by the number of electrons $Z$ in an atom. At such photon energies three distinct mechanisms contribute significantly to the attenuation of X-ray beams, namely the photoelectric effect, elastic scattering and inelastic (Compton) scattering [2].

Figure 3 further shows the mass attenuation coefficients for thermal neutrons, e. g. a common spectrum centred around $\approx 25$ meV neutron energies (triangles). The trend is much less obviously a function of $Z$ than in case of X-rays which is because the predominant nuclear interaction depends on the internal configuration of a nucleus and not just the number of protons $Z$. As for X-rays, various mechanisms can remove neutrons from an incident beam, namely direct nuclear absorption, (quasi)elastic scattering, inelastic scattering and magnetic scattering [2].

In summary, the X-rays interact with the electrons while the neutrons with the nucleus of the atom. As the interactions are different, complementary use of X-ray and neutrons in imaging, (see e. g. [2, 16, 22–24]) as well as in diffraction and scattering, will provide additional information.

## 3. Requirements for successful imaging

A typical setup for tomographic imaging consists of a rotation and translation stage, a scintillator screen, optics including a deflecting mirror and a charge coupled device

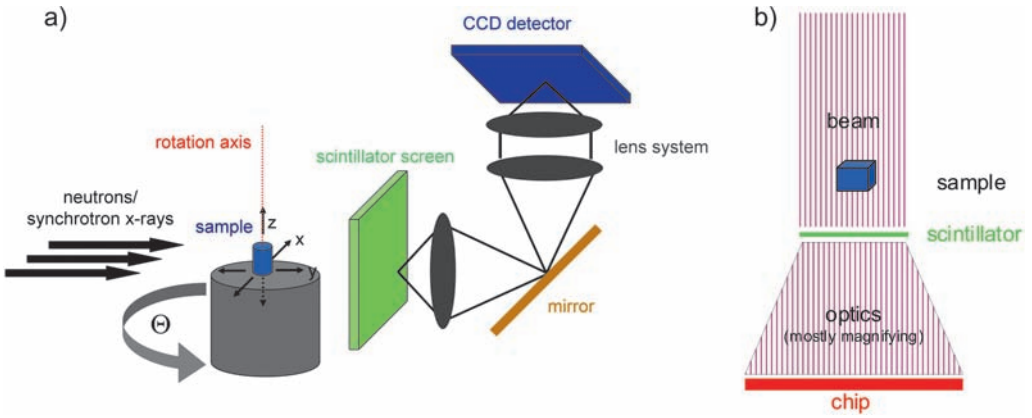


Fig. 4. (a) schematic layout of a tomography experiment. (b) factors influencing imaging quality.

(CCD) camera, see Fig. 4. Going downstream from the radiation source, each component has to be optimised appropriately.

The quality of the incoming beam is a limiting factor of imaging. The beam divergence has to be reduced below a given level by appropriate collimation. Especially for neutrons, there is a trade-off between flux reduction and beam collimation expressed by the $L/d$ ratio ($L$ = distance aperture to detector, $d$ = aperture diameter) that is rarely pushed to above 500 [2].

The mechanical components have to ensure that the beam path is stable, reproducible and free of fluctuations due to thermal and mechanical disturbances. The alignment of the rotation axis is crucial especially for high resolution synchrotron X-ray tomography [2].

The scintillator screen converts the incoming X-ray photons or neutrons to visible light. Since each impinging photon or neutron creates light emerging from a small disc there is an adverse effect on spatial resolution. Scattering within the scintillator material further creates a halo around the point of incidence. Currently, the scintillator materials in use define a lower limit for resolution which is around 0.5 µm and 20 µm for X-rays and neutrons, respectively [2, 25]. Another important aspect is conversion efficiency and in many cases a trade-off between resolution and efficiency has to be sought.

The optics used to project the scintillator image onto the camera chip – mostly a CCD – also limits the spatial resolution. As the wavelength of the visible light produced is around 0.5 µm diffraction already defines a lower limit. Aberrations further contribute.

The device that converts the projected image into a digital image provides further limitations due to spatial resolution (pixel size) and efficiency. The pixel size of such a device is related to spatial resolution of the entire setup only when none of the other components dominates resolution. For example, when a point-like feature in the sample is blurred by the scintillator, after which the optics magnify this blur to more than the size of one pixel, the blur will be smeared out over various pixels and no resolution is gained.

Another aspect is the time resolution of the detector system. The afterglow of the scintillating screens – that can be in the range of µs to ms – normally does not influence the quality of the image in standard imaging experiments where the exposure times range from several 10 ms to seconds. In the case of dynamic imaging, afterglow could limit measurement speed and quality. High-speed Complementary Metal–Oxide–Semiconductor (CMOS) detectors allow for very short exposure times (ns). However it is the readout time which limits the performance to typically some 1 000 frames per second. Improvement of the speed can be obtained by using binning in one or two directions. In this case dynamical processes can be investigated with a time resolution of some hundred µs. Of course the available flux density should allow for the use of these short exposure times. On the other hand real time imaging is possible in the case of white beam synchrotron radiation. The very short exposure times allow for high-speed tomography investigations where a fully tomographic experiment below 1 s is possible. Of course the data storage and data management problem is another limitating factor which should be considered. As the neutron sources do not have the brilliance of synchrotron radiation, a stroboscopic technique is usually used where an average image of the process can be obtained.

## 4. Applications

### 4.1. Applications exploiting the complementarity of photons and neutrons

In the following section examples are given which show the range of scientific questions in material science and engineering where synchrotron and neutron tomography can be usefully employed. A review about application of X-ray microtomography in materials science can be found in [2]. Here the complementarity of tomography using X-rays and neutrons is emphasized and illustrated regarding different aspects: spatial resolution, sensitivity to hydrogen and to contrast agents.

#### 4.1.1. Imaging of phases in a metallic foam

Since neutron tomography is very sensitive to hydrogen, it is very often used to complement X-ray tomographic measurements and to reveal the hydrogen distribution in different materials. As an example two tomograms of a metallic aluminium foam [26–28] (AlSi6Cu4) are given in Fig. 5. Aluminium foams are produced in a first step as precursor materials where a blowing agent – typically $TiH_2$ – is added. The distribution of the blowing agent before and after foaming is an important issue in foam development. While X-ray tomography is very useful for displaying the microstructure with adequate spatial resolution (Fig. 5a),

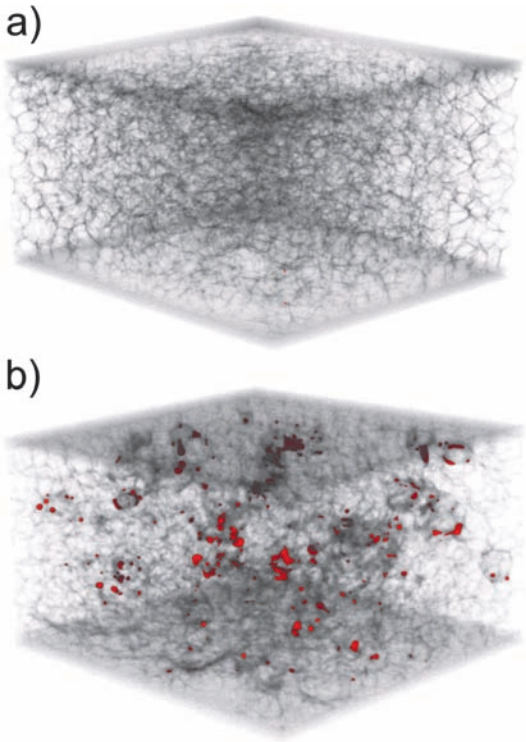


Fig. 5. X-ray (a) and (b) neutron tomography of an AlSi6Cu4 foam. $TiH_2$ agglomerations in red.

neutron tomography was used to reveal the local $TiH_2$ agglomerations (appearing in red in Fig. 5b) [29].

### 4.1.2. Water management of fuel cells

One of the main applications of neutron and synchrotron X-ray in-situ imaging in applied sciences and industrial research is the investigation of fuel cells and their components/materials. In low temperature PEM (polymer electrolyte membrane) fuel cells, liquid water plays a crucial role [30–44]. On the one hand, a certain amount of liquid water is necessary, because only a wet membrane is proton conductive while a dry polymer membrane changes its structure and the electric conductivity of the membrane collapses [32]. On the other hand, flooding of gas transport (flow field) channels and porous gas diffusion layers (GDLs) severely affects the achievable power densities and the longevity of the components [32]. Liquid water hinders the transport of reactant and product gases ($O_2$, $H_2$) and hence the supply of the catalysts with reactive gases. Thus, well-balanced water management at any operating and environmental conditions is important for efficiency and lifetime of PEM fuel cells [32, 45].

Neutron and synchrotron X-ray radiography are unique methods to investigate the liquid water distribution in a fuel cell while at the same time applying realistic power profiles and environmental conditions. Neutrons penetrate the metallic components of the cells easily and are sensitive to water; hence they are used to investigate entire cells (Fig. 6a), as they are employed in different applications, often without the necessity to adapt the cell components to the imaging instrument. On the other hand synchrotron X-ray radiography allows for high spatial resolutions around 1 µm and fast imaging with time resolutions of some

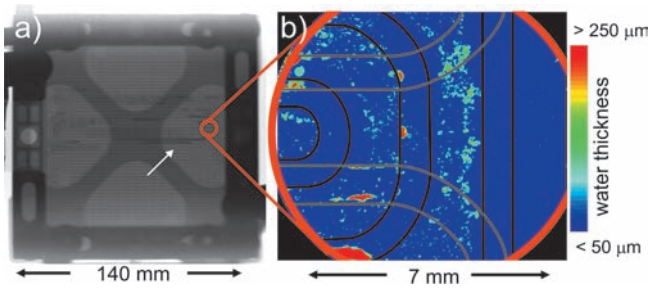


Fig. 6. Two radiograms of a low temperature PEM fuel cell taken with (a) neutrons and (b) synchrotron X-rays. The synchrotron radiogram shows a small area of the cell where a hole was drilled into the metallic end plate of the fuel cell [35].

100 ms. However, holes have to be drilled into the metallic cases/end plates of the fuel cells to ensure that no metallic parts are attenuating the beam. Figure 6b shows a radiogram where small water droplets of a few µm in size can be seen. Details of the very early stages of water development are revealed. For example, the water development process starts below the flowfield channels as predicted by simulations [34, 35].

### 4.1.3. Time evolution of battery discharge

Another example for the complementary use of neutron and synchrotron X-ray imaging is given in Fig. 7. The images show cross-sections through tomograms of alkaline batteries taken with synchrotron X-rays (a and b) and neutrons (c and d) before (images a and c) and after (b and d) discharge. The X-ray tomogram reveals structural changes of the zinc powder (white particles in the centre) that is oxidised and partly dissolved in the KOH electrolyte [46]. The cathode is swelling and cracking due to the reduction of $MnO_2$ (grey area) and the intercalation of hydrogen (Fig. 7b). The latter can not be visualised with X-rays.

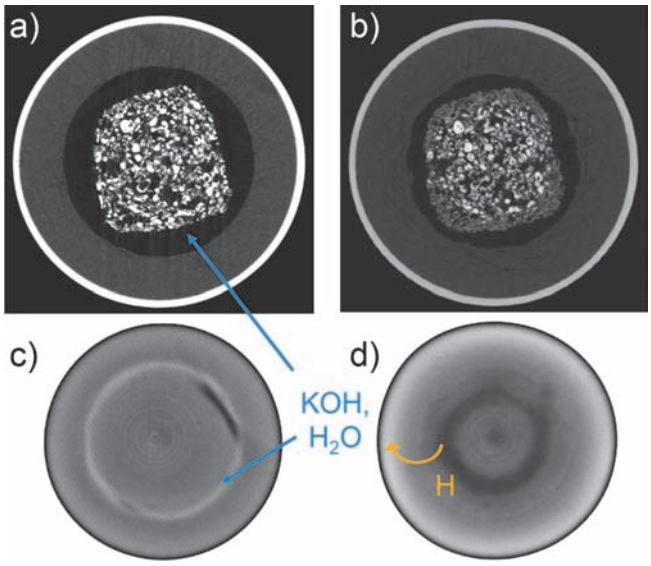


Fig. 7. Cross-sections through the tomograms of alkaline batteries. (a) and (b) synchrotron tomography of an AAA battery and (c) and (d) neutron tomography of a C-block size battery. (a) and (c) were taken before and (b) and (d) after discharge. The diameter of the battery in (a) and (b) was 8.2 mm, that in (c) and (d) 26 mm [23].

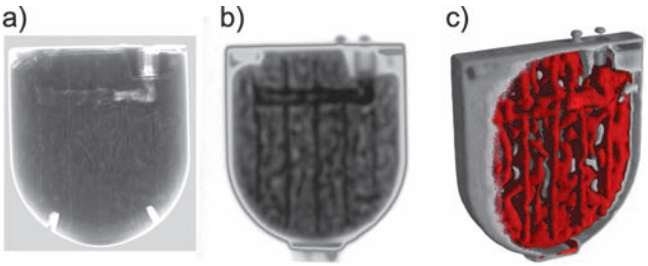


Fig. 8. Lithium iodide battery: (a) X-ray radiogram that shows mainly the iodine distribution, (b) neutron radiogram that displays the Li distribution in the same battery. (c) neutron tomogram, the battery housing was partly cut in the tomogram to open the view on the Li distribution (red). The width of the battery is 27 mm [19].

However, neutrons were used to investigate a comparable battery in order to analyse the hydrogen transport (Fig. 7d). It was found that after discharge hydrogen has moved from the electrolyte (dark areas) into the $MnO_2$ (bright areas) [23]. This example demonstrates how the different contrasts achieved with X-rays and neutrons are complementing each other.

The complementary properties of X-rays and neutrons are also very well suited to investigating lithium batteries. As an example an investigation of a lithium-iodide battery is given in Fig. 8. Because of their solid state electrolyte LiI this battery type provides very high reliability and limited short-circuit currents that makes it suitable for many medical applications, especially for pacemakers. Iodine is a classical contrast agent in X-ray imaging and lithium a typical screening and scintillator material in neutron imaging. Hence X-rays and neutrons are ideally suited complementary probes which allow imaging the distribution of lithium and iodine in two separate measurements [19]. In this way the stability of the LiI electrolyte over long time periods was investigated, and the images revealed a strong change in the lithium distribution after several years. This gives important hints for the developers to optimise the lifetimes of the batteries with the aim to extend their exchange intervals and thus to limit the number of necessary surgeries.

### 4.2. Emerging techniques

Methods development in synchrotron X-ray and neutron tomography aims at obtaining higher spatial resolution, time resolution as well as increasing contrast e. g. between phases or materials, see e. g. Refs. [2, 13, 14, 16, 47–52].

#### 4.2.1. High-flux white beam tomography

In many cases it is desirable to investigate changes in sample with both 3D spatial and temporal resolution. This makes X-ray and neutron beams with very high fluxes necessary to ensure that a tomogram can be performed within a short time. X-ray tomographic measurements within a few seconds have become feasible using a white X-ray beam, see Fig. 9a, for an example obtained at the BESSY storage ring and references for other developments described in the literature [53–58]. To accelerate imaging – especially for neutrons – beam collimation can be reduced at the cost of spatial resolution. Despite the comparably low available fluxes at neutron

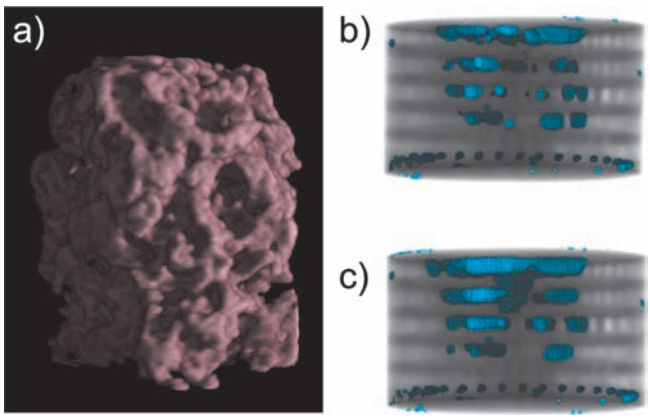


Fig. 9. Fast white beam tomography. (a) 3D view on a white beam synchrotron X-ray tomogram of a porous steel foam taken within 15 s (EDDI beamline at HZB). (b) and (c) are neutron tomograms of a small fuel cell which were taken within 15 min. (CONRAD/V7 at HZB). Time between the two measurements was 45 min. In the tomogram (c) about twice as much water was found as in (b) caused by changes in the operating parameters.

tomography facilities, tomographic measurements within a few minutes have become possible. Figure 9b and c shows two tomograms that were taken within 15 min and that show the development of the water distribution in a small fuel cell. Such small fuel cells might serve as replacement for D-block batteries in future. Because of the slow water flow, time resolution is sufficient in this case.

In order to investigate time-dependent processes with synchrotron X-rays, work was oriented towards the use of high flux insertion devices delivering a broad energy spectrum, which led to the development of fast-tomography setups capable of collecting a full 3-D dataset in less than one second [59]. The white high-energy X-ray beam used does not have any temporal coherence, but due to the small source size it remains transversally coherent. Phase-contrast tomography can therefore be performed at the same speed as absorption contrast tomography. The absorbed dose is usually small due to the small X-ray absorption at high energies, which allows for the measurement of systems sensitive to radiation damage such as biological sam-

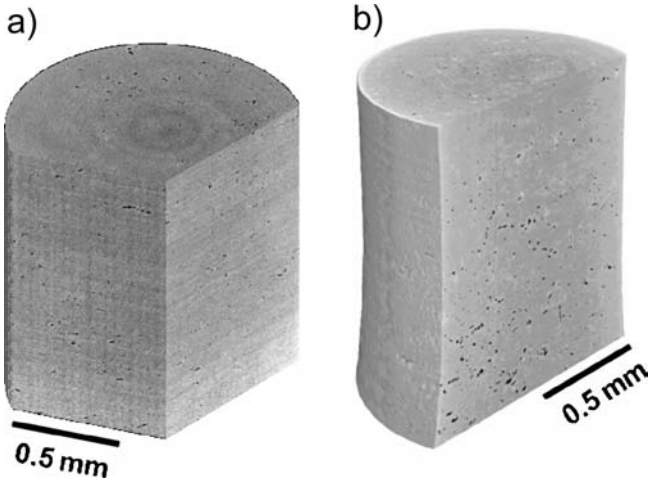


Fig. 10. Damage distribution in (a) Oxygen free high conductivity (OFHC) copper and (b) Cu-40Zn-2Pb brass alloy at the beginning of tertiary creep.

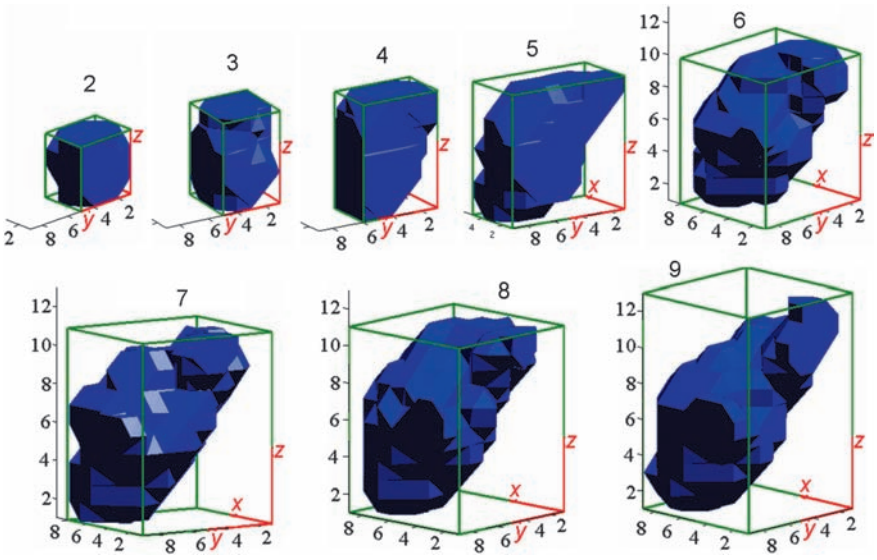


Fig. 11. Example of cavity shape evolution in Cu-40Zn-2Pb brass alloy. The units are given in voxels (1 voxel = $1.6^3$ µm$^3$).

ples. High energy radiation, however, is detrimental to the spatial resolution of fast-tomography setups, because due to the low efficiency of the available scintillator materials (YAG:Ce, LAG:Eu), relatively thick scintillators have to be used [54].

Fast-tomography has been successfully applied to in-situ investigation of steel powder compacts during sintering [60], as well as to study the coarsening of dendritic arms during solidification of an aluminium alloy [61]. Due to its 4D character in situ tomography is well adapted to damage characterisation during plastic deformation. Maire et al. [57] have shown a good correlation between damage determined by in situ tomography and acoustic emission. Damage during high temperature creep of metallic materials was the subject of several other works [53, 62, 63]. A picture of damage distribution in creep deformed copper and brass alloy is shown in Fig. 10. The damage process consists of three concurrent mechanisms: nucleation, growth and coalescence of grain boundary voids, which cannot be easily separated. Fast-tomography coupled with image analysis allows a conceptually new approach to damage evaluation. It allows following the evolution of single voids from the detection limit until coalescence [62, 63]. This avoids per se the effect of nucleation and based on ancestor analysis and shape of the voids the coalescence effect can also be minimised. An example of cavity evolution in brass is shown in Fig. 11. The cavity is aligned at 45° to the tensile vertical axis, suggesting that grain boundary sliding mechanism might be responsible for its growth.

According to the continuum theory describing the growth-rate of a void in a creeping nonlinearly viscous solid a pure proportionality is expected between the growth-rate $\dot{V}$ and actual cavity volume $V$ [64]:

$$\dot{V} = \Lambda \dot{\varepsilon} V \qquad (1)$$

where $\dot{\varepsilon}$ is the strain-rate and the parameter $\Lambda$ equals 3/4 and is about unity for a spherical void in a deforming linear and nonlinear viscous material, respectively [64]. Experimental results of [62, 63] as well as the data in Fig. 12 indicate that the growth rate of cavities in copper with an equivalent cavity radius in the range of 2.0–5.1 µm follows the predicted functional form; however, the factor $\Lambda$ is much

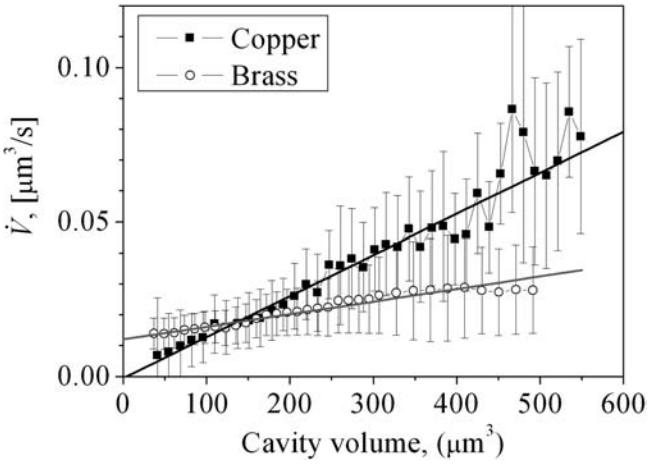


Fig. 12. Cavity growth rates in OFHC copper and α/β brass as a function of cavity volume. The line fitting the brass data has a positive intercept indicating the presence of a growth mechanism in addition to plastic creep.

larger ($\Lambda \sim 45$ for copper) than predicted by e. g. Riedel [65] ($\Lambda \sim 1.1$). The large standard deviations (shown as error bars), however, indicate a that there is a large variety of growth rates for voids of the same size, which presumably can be linked to the local neighbourhood of the voids (such as crystallography of neighbour grains) as well as to the geometry aspect of the void shape.

### 4.2.2. Magnetic imaging

Due to their intrinsic magnetic moment neutrons are sensitive to magnetic fields and hence neutron radiography and tomography can be used to investigate magnetic field distributions [66–68]. For this purpose a neutron polariser and an analyser are added to a neutron imaging set-up. Polariser and analyser are placed into the beam in front of and behind the sample, respectively (compare Fig. 4). A magnetic field in a sample causes a precession of the neutron spin around the field axis. The total angle of precession depends on the strength of the field and on the time that the neutron spends within the field. The rotation angle can be measured and the

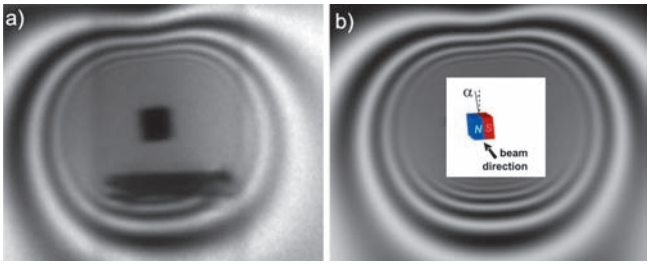


Fig. 13. (a) Polarised neutron radiogram of a permanent magnet levitating over a Yttrium barium copper oxide (YBCO) superconductor. (b) corresponding simulated image. The inset shows the orientation of the dipole as derived from the fitting procedure [66].

field strength along the path calculated. Figure 13a shows a polarised neutron radiogram of a permanent magnet levitating over a YBCO superconductor cooled by liquid nitrogen. The rings around the magnet are caused by the decreasing strength of the magnetic field with increasing distance to the magnet (but they do *not* represent field lines). The neutron spin-state "beats" between spin-up and spin-down. A dark line indicates an anti-parallel orientation of the measured spin state with respect to the initial spin state and a white line a parallel orientation. A simulation of the experiment and a successive fitting procedure reveals that the dipole magnet was orientated as shown in the inset in Fig. 13b, with $\alpha = 4^\circ$ (tilting angle to the horizontal plane).

### 4.2.3. Phase contrast imaging

In many cases image contrast can be strongly increased by so-called phase contrast radiography/tomography [69–71]. When the distance between sample and detector is increased, Fresnel-propagation introduces interference fringes at material interfaces and boundaries. These fringes are used to visualise the interfaces in 2D and 3D. Two examples are given in Fig. 14. First a pair of human hairs was measured with synchrotron X-ray radiography at sample-detector distances of 20 mm (a), 500 mm (b) and 1 100 mm (c) respectively. At very close distances practically no such effects are visible and the projection image mainly depends on the pure attenuation of the sample that gives a weak contrast in this case. With increasing distance the effect becomes visible and more pronounced. Phase contrast imaging is also possible with neutrons, as shown

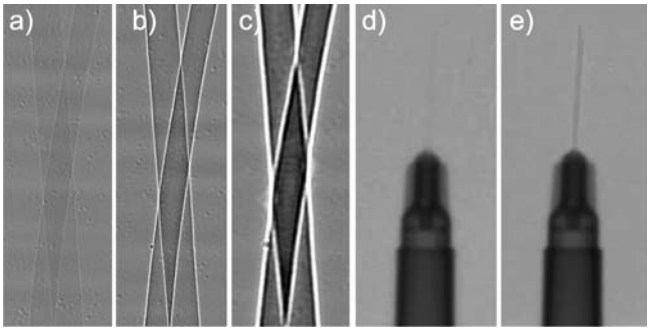


Fig. 14. (a), (b) and (c) Synchrotron X-ray, and (d) and (e) neutron phase contrast radiographies taken at different detector-sample distances [72].

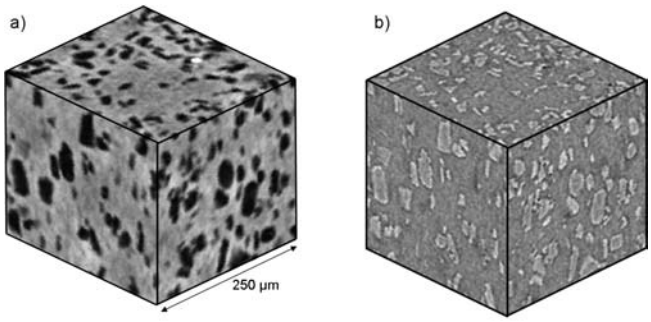


Fig. 15. (a) Holotomography and (b) phase-contrast tomography reconstructions of a metal-matrix composite consisting of aluminium matrix and 20 vol.% $Al_2O_3$ particles.

in Fig. 14, where a steel needle was measured at 5 mm and 700 mm sample-to-detector distance.

When a commonly used tomographic reconstruction algorithm, such as filtered back projection is applied to a set of phase contrast radiographies, the resulting tomogram displays all interfaces and boundaries within the material in 3D. However, artefacts sometimes prevent quantitative analysis of the data.

The high brilliance and partial coherence of a synchrotron X-ray beam allows for the detection of the real part of the refractive index (holotomography), which could significantly increase image contrast [47, 72]. Phase retrieval algorithms can be applied to one (in the case of a homogeneous material with known attenuation coefficient) – or most commonly three or four – phase contrast radiographies in order to calculate a so called phase map, which displays the local phase shift instead of the beam attenuation [73]. From a set of phase maps taken at different rotation angles of the sample a holotomogram can be reconstructed that yields an increase in contrast by up to three orders of magnitude compared to (conventional) absorption contrast tomography [47, 72].

The holotomographic reconstruction of a metal-matrix composite consisting of $Al_2O_3$ particles embedded in aluminium matrix is shown in Fig. 15a. Compared to absorption or phase contrast reconstructions the grey level separation of the two constituting phases is much larger, which allowed a simple segmentation of the reconstruction and a proper characterisation of the size, shape and spatial distribution of ceramic particles [74]. The structure obtained with holotomography could be directly imported into finite element models used for predicting the effective properties of the real composite [75].

### 4.2.4. Differential phase and dark-field contrast tomography

Besides propagation based phase contrast discussed above, differential phase contrast is a well suited tool to address the refractive index distribution of samples. Differential phase contrast methods measure the refractive angular beam deviations that lead to intensity variations in the propagation based method (Fig. 16). This naturally requires high angular resolution like it can be achieved in double crystal diffractometer instruments (DCD) [76]. Consequently, such set-ups have been used with X-rays and neutrons for differential phase contrast tomography referred to

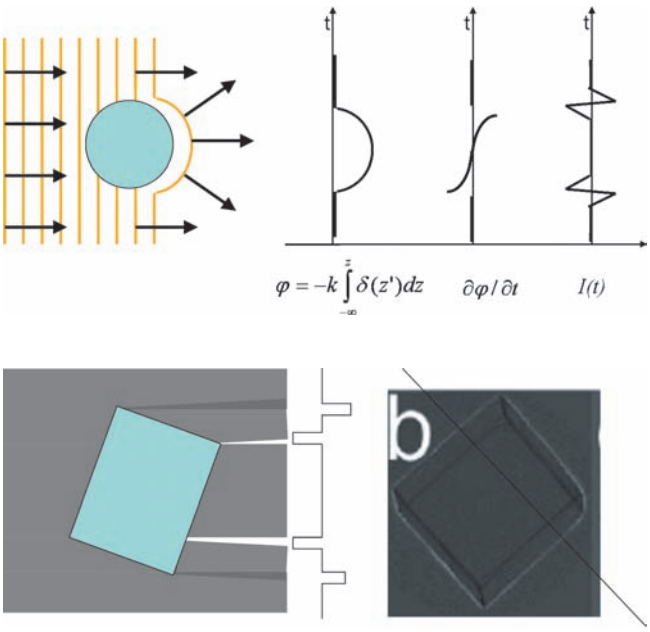


Fig. 16. Schematic representation of the formation of phase contrast with respect to phase, refraction angle and intensity variation and a comparison of a schematic representation of the contrast according to the propagation based technique in a cross-section.

as diffraction enhanced imaging (DEI) or refraction contrast [77–84]. However, due to the limited phase space density of neutrons and X-rays from low brilliance sources, the high coherence conditions in a DCD oppose a broad application at these sources. A more efficient alternative method for differential phase contrast was introduced utilizing a grating interferometer set-up capable to decouple spatial resolution form angular resolution despite of loose coherence conditions [85]. This method, based on a phase grating producing a fringe pattern beyond the spatial resolution of the detector, which can be analysed stepwise by an absorption grating in front of the detector, can be used efficiently even at low-brilliance sources, when it is combined with a source grating providing partially coherent beams [86, 87].

Both types of instruments can, due to their high angular resolution, be utilized for the spatial resolved detection of ultra-small angle scattering (USAS) as well. Ultra small angle scattering provides information about structures in the sample in a size range beyond the direct spatial resolution. This information can be extracted from the same measurements addressing attenuation and phase contrast as well. The usefulness of this information has been demonstrated in various X-ray [88, 89] and neutron DCD measurements. Notably the first tomography has been provided with neutrons, despite the low flux density in such instruments [90] (Fig. 17a). However, also for this kind of investigations the grating interferometer is superior and enables investigations on more reasonable timescales for three-dimensional spatial resolution even at laboratory X-ray sources [91] and with neutrons [92] (Fig. 17b–d). The method is mainly called dark-field imaging but is also referred to as e. g. USAS- or extinction contrast.

The magnetic moment of the neutron additionally enables to achieve differential phase and dark-field contrast from magnetic fields and structures. Magnetic fields add a spin dependent refractive index contribution and hence magnetic field gradients induce spin dependent angular beam deviations e. g. at domain walls. First dark-field imaging of magnetic domains in a DCD was reported as early as in 1989 [94, 95] (Fig. 18a). With polarised neutrons, respec-

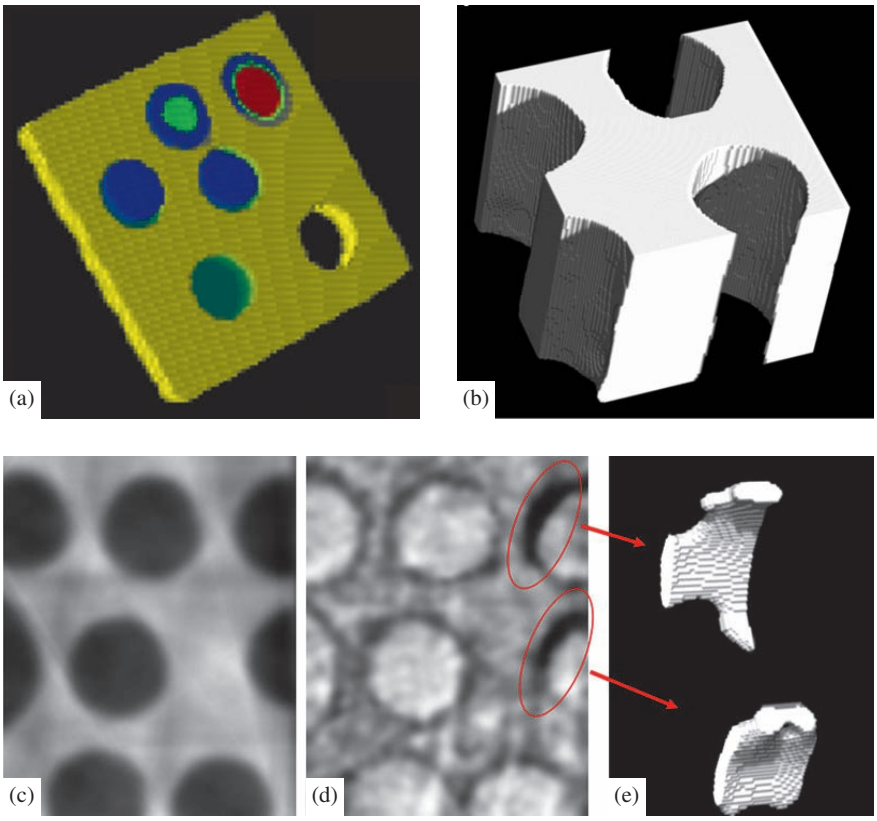


Fig. 17. Differential phase (refraction) contrast reconstruction slice of a $2 \times 2 \times 3$ cm$^3$ Al matrix combined with a dark-field (USANS) reconstruction of beta-carotene in $D_2O$ in the holes of the matrix (single slice) from DCD data (a) [98]; a 3-dimensional dark-field contrast reconstruction of an Al matrix with holes of 4 mm diameter and of sediments in corresponding holes from grating interferometer data (b, e, respectively) [92]; refraction and dark field reconstruction of a corresponding slice of the same sample (c, d).

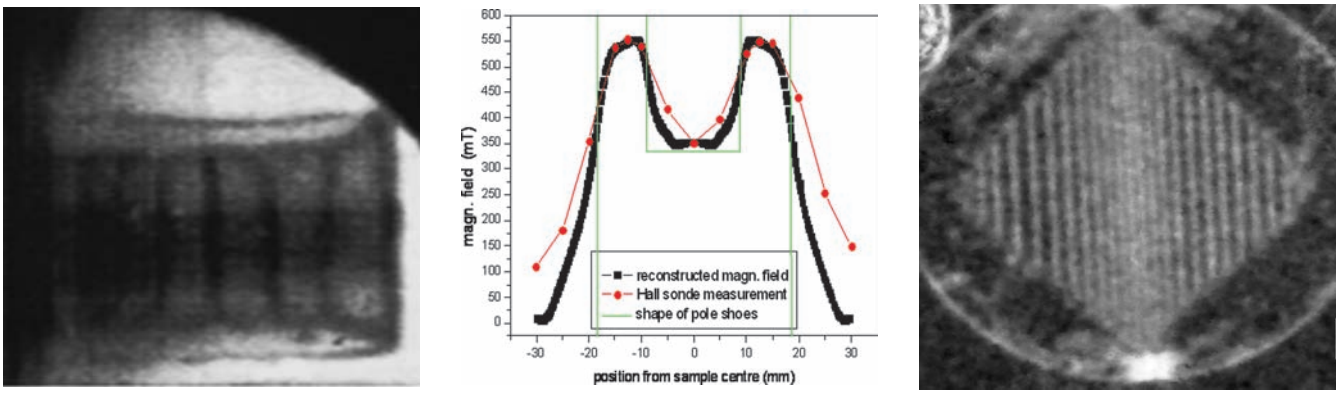


(a) (b) (c)

Fig. 18. Visualisation of magnetic domain walls in FeSi single crystal cylinder with a diameter of 13 mm in a DCD (a) [95]; line profile of the cross-section of a magnetic field between two pole-shoes as reconstructed from DCD measurements compared to hall probe measurements (b) [96]; visualisation of Bloch walls in a thin FeSi plate recorded with a grating interferometer (c) [97].

tively polarisation analyses quantitative reconstructions of cross-sections of magnetic fields have been achieved using the same method [96] (Fig. 18b). Polarisation was, however, not necessary to visualize Bloch walls between magnetic domains where the spin states of an unpolarised beam split by different refraction angles and hence provide a dark-field-like signal. The application of the more efficient grating interferometer set-up for this purpose is promising for further applications like has been demonstrated recently [97] (Fig. 18c).

## 5. Outlook

The development of imaging methods based on neutrons and synchrotron X-rays is still under way. Neutron imaging especially is a latecomer and therefore the potential for novel experimental options is large. Very soon, 10 µm will be a standard resolution in neutron absorption tomography which would provide complementarity with conventional X-ray tomography based on microfocus X-ray tubes. For even higher resolutions, advanced concepts such as neutron lenses or neutron mirrors would be required. Such developments are on the way [98] but no successful high-resolution experiment has been carried out so far. Moreover, the exploitation of the magnetic moment of the neutron either in polarised imaging experiments or experiments on magnetic materials holds the promise of many fruitful developments. On the synchtrotron X-ray side, the spatial resolution of direct projective imaging is intrinsically limited by the scintillation process. Major developments go towards hard X-ray microscopes based on bent mirror or X-ray lens systems. Such experiments have already been carried out. The time resolution of X-ray tomography could be further improved, but the heat load on the sample by the beam and the enormous amount of data associated with sequences of tomographic data present major challenges.

Both neutron and synchrotron X-ray tomographic methods hold enormous potential both for basic and applied research in various scientific areas in engineering materials research. In particular, they are increasingly relevant to material and device development for energy technologies and transport applications. Progress in instrument and method development also provides benefits for research in other disciplines such as art and archaeology, chemical process technology or production technologies.

### References

[1] C.-O. Fischer, in: J.B. Barton (Eds.), Neutron Radiography, (Proc. 4th World Conference, 10.–16. May 1992, San Francisco, USA), Gordon and Breach, Chemin de la Sallaz, CH (1994) 213.
[2] S.R. Stock: International Materials Reviews, 53 (2008) 129–181. DOI:10.1179/174328008X277803
[3] J.H. Kinney, M.C. Nichols: Annual Review of Materials Science 22 (1992) 121–152. DOI:10.1146/annurev.ms.22.080192.001005
[4] B.P. Flannery, H.W. Deckman, W.G. Roberge, K.L. D'amico: Science 237 (4821) (1987) 1439–1444.
[5] J. Banhart (Ed.): Advanced Tomographic Methods in Materials Research and Engineering, Oxford University Press, Oxford, UK (2008).
[6] J. Baruchel, P. Bleuet, A. Bravin, P. Coan, E. Lima, A. Madsen, W. Ludwig P. Pernot, J. Susini: Advances in Synchtron Hard X-ray Based Imaging, Comptes Rendus Physique 9 (2008) 624. DOI:10.1016/j.crhy.2007.08.003
[7] J. Baruchel, J.-Y. Buffiere, P. Cloetens, M. Di Michiel, E. Ferrie, W. Ludwig, E. Mair, L. Salvo: Advances in Synchrotron Radiation Microtomography, Scripta Materialia 55 (2006) 41. DOI:10.1016/j.scriptamat.2006.02.012
[8] S.R. Stock: Proceedings of SPIE: Developments in X-Ray Tomography VI – Introduction (2008) 7078.
[9] L. Grodzins: NIM B 206 (3) (1983) 547. DOI:10.1016/0167-5087(83)90394-0
[10] U. Bonse, F. Beckmann, M. Bartscher, T. Biermann, F. Busch, O. Günnewig: Proceedings of SPIE – The International Society for Optical Engineering 3149 (1997) 108.
[11] C. Hall, P. Barnes, J.K. Cockcroft, S.L. Colston, D. Häusermann, S.D.M. Jacques, A.C. Jupe, M. Kunz: NIM B 140 (1998) 253. DOI:10.1016/S0168-583X(97)00994-4
[12] J.H. Kinney, M.C. Nichols: Annual Review of Materials Science 22 (1992) 121. DOI:10.1146/annurev.ms.22.080192.001005
[13] E. Maire, J.-Y. Buffière, L. Salvo, J.J. Blandin, W. Ludwig, J.M. Létang: Advanced Eng. Mat. 3 (2001) 539. DOI:10.1002/1527-2648(200108)3:8<;539::AID-ADEM539>3.0.CO;2-6
[14] J. Baruchel, J.-Y. Buffière, P. Cloetens, M. Di Michiel, E. Ferrie, W. Ludwig, E. Maire, L. Salvo: Scripta Mat. 55 (2006) 41. DOI:10.1016/j.scriptamat.2006.02.012
[15] F. Beckmann, R. Grupp, A. Haibel, M. Huppmann, M. Nöthe, A. Pyzalla, W. Reimers, A. Schreyer, R. Zettler: Advanced Eng. Mat. 9 (2007) 939. DOI:10.1002/adem.200700254
[16] W. Reimers, A. Pyzalla, A. Schreyer, H. Clemens (Eds): Neutrons and Synchrotron Radiation in Engineering Materials Science, Wiley-VCH, Weinheim (2008).
[17] P. Vontobel, E.H. Lehmann, R. Hassanein, G. Frei: Physica B: Condensed Matter 385–386 I (2006) 475.

[18] A.S. Tremsin, J.V. Vallerga, J.B. McPhate, O.H.W. Siegmund, J.S. Hull, W.B. Feller, L. Crow, R.G. Cooper: IEEE Nuclear Science Symposium Conference Record, 1, Article No. 4436329 (2007) 270.
[19] M. Strobl, I. Manke, N. Kardjilov, A. Hilger, M. Dawson, J. Banhart: J. Physics D: Applied Physics 42 (2009) 243001. DOI:10.1088/0022-3727/42/24/243001
[20] V.V. Nagarkar, D. Penumadu, I. Shestakova, S.C. Thacker, S.R. Miller, J.F. Ankner, H.Z. Bilheux, C.E. Halbert: IEEE Transactions on Nuclear Science 56 (4) (2009) Article No. 5204674, 2493.
[21] P. Boillat, G. Frei, E.H. Lehmann, G.G. Scherer, A.Wokaun: Electrochemical and Solid-State Letters 13 (2010) B 25. DOI:10.1149/1.3279636
[22] F. Beckmann, J. Vollbrandt, T. Donath, H.W. Schmitz, A. Schreyer: NIM A 542 (2005) 279. DOI:10.1016/j.nima.2005.01.148
[23] I. Manke, J. Banhart, A. Haibel, A. Rack, S. Zabler, N. Kardjilov, A. Hilger, A. Melzer, H. Riesemeier: Appl. Phys. Lett. 90 (2007) 214102. DOI:10.1063/1.2742283
[24] D. Mannes, P. Niemz, E. Lehmann: Wood Research 54 (3) (2009) 33.
[25] E.H. Lehmann, G. Frei, G. Kühne, P. Boillat: NIM A 576 (2007) 389. DOI:10.1016/j.nima.2007.03.017
[26] H.-P. Degischer, B. Kriszt (Eds.): Handbook of Cellular Metals and Metal foaming Technology (MIT-Verlag, Bremen, 2001).
[27] B. Kriszt, B. Foroughi, K. Faure, H.-P. Degischer, in: J. Banhart, M.F. Ashby, N.A. Fleck (Eds.), Metal Foams and Porous Metal Structures, MIT-Verlag, Bremen, (1999) 241.
[28] R. Jancek, A. Kottar H.-P. Degischer, in: J. Banhart, N.A. Fleck, A. Mortensen (Eds.), Cellular Metals – Manufacture, Properties, Applications, MIT-Verlag, Berlin (2003) 19.
[29] F. Garcia-Moreno, C. Jimenez, M. Mukherjee, V. Kumar, G. Sanjeeviah, I. Manke, A. Hilger, N. Kardjilov, J. Banhart, G. Schumacher, Ch. Genzel, M. Tovar: Proceedings of Metfoam (2009) submitted.
[30] A.B. Geiger, A. Tsukada, E. Lehmann, P. Vontobel, A. Wokaun, G.G. Scherer: Fuel Cells, 2 (2002) 92. DOI:10.1002/fuce.200290007
[31] P. Boillat, D. Kramer, B.C. Seyfang, G. Frei, E. Lehmann, G.G. Scherer, A. Wokaun, Y. Ichikawa, Y. Tasaki, K. Shinohara: Electrochem. Comm. 10 (2008) 546. DOI:10.1016/j.elecom.2008.01.018
[32] C.Y. Wang: Chem. Rev. 104 (2004) 4727. PMid:15669167; DOI:10.1021/cr020718s
[33] R.J. Bellows, M.Y. Lin, M. Arif, A.K. Thompson, D. Jacobson: J. Electrochem. Soc. 146 (1999) 1099. DOI:10.1149/1.1391727
[34] C. Hartnig, I. Manke, R. Kuhn, N. Kardjilov, J. Banhart, W. Lehnert, Appl. Phys. Lett. 90 (2008) 134106. DOI:10.1063/1.2907485
[35] I. Manke, C. Hartnig, M. Grünerbel, W. Lehnert, N. Kardjilov, A. Haibel, A. Hilger, H. Riesemeier, J. Banhart: Appl. Phys. Lett. 90 (2007) 174105. DOI:10.1063/1.2731440
[36] I. Manke, C. Hartnig, N. Kardjilov, M. Messerschmidt, A. Hilger, M. Strobl, W. Lehnert, J. Banhart: Appl. Phys. Lett. 92 (2008) 244101. DOI:10.1063/1.2946664
[37] A. Bazylak, D. Sinton, Z.-S. Liu, N. Djilali, Journal of Power Sources 163 (2007) 784–792. DOI:10.1016/j.jpowsour.2006.09.045
[38] M.A. Hickner, N.P. Siegel, K.S. Chen, D.N. McBrayer, D.S. Hussey, D.L. Jacobson, M. Arif: J. Electrochem. Soc. 153 (2006) A902–A908. DOI:10.1149/1.2184893
[39] A. Turhan, K. Heller, J.S. Brenizer, M.M. Mench: J. Power Sources 160 (2006) 1195–1203. DOI:10.1016/j.jpowsour.2006.03.027
[40] M.A. Hickner, N.P. Siegel, K.S. Chen, D.S. Hussey, D.L. Jacobson, M. Arif: J. Electrochem. Soc., 155 (2008) 427.
[41] R. Satija, D.L. Jacobson, M. Arif, S.A. Werner: J. Power Sources 129 (2004) 238–245. DOI:10.1016/j.jpowsour.2003.11.068
[42] J.P. Owejan, T.A. Trabold, D.L. Jacobson, D.R. Baker, D.S. Hussey, M. Arif: Int. J. Heat Mass Transfer 49 (2006) 4721–4731. DOI:10.1016/j.ijheatmasstransfer.2006.07.004
[43] C. Hartnig, I. Manke, J. Schloesser, P. Krüger, R. Kuhn, H. Riesemeier, K. Wippermann, J. Banhart: Electrochem. Comm. 11 (2009) 1559. DOI:10.1016/j.elecom.2009.05.047
[44] I. Manke, C. Hartnig, M. Grünerbel, J. Kaczerowski, W. Lehnert, N. Kardjilov, A. Hilger, W. Treimer, M. Strobl, J. Banhart: Appl. Phys. Lett. 90 (2007) 184101. DOI:10.1063/1.2734171
[45] W. Schmittinger, A. Vahidi: J. Power Sources 180 (2008) 1–14. DOI:10.1016/j.jpowsour.2008.01.070
[46] Q.C. Horn, Y. Shao-Horn: J. Electrochem. Society 150 (2003) 652. DOI:10.1149/1.1566014
[47] P. Cloetens, W. Ludwig, J. Baruchel, D. Van Dyck, J. Van Landuyt, J.P. Guigay, M. Schlenker: Appl. Phys. Lett., 75 (1999) 2912. DOI:10.1063/1.125225
[48] P. Cloetens, M. Pateyron-Salomé, J.Y. Buffière, G. Peix, J. Baruchel, F. Peyrin, M. Schlenker: J. Appl. Phys. 81 (1997) 5878. DOI:10.1063/1.364374
[49] G.C. Requena, H.-P. Degischer, E.D. Marks, E. Boller: Mat. Sci. Eng. A 487 (2008) 99. DOI:10.1016/j.msea.2007.10.016
[50] G.C. Requena, P. Cloetens, W. Altendorfer, C. Poletti, D. Tolnai, F. Warchomicka, H.-P. Degischer: Scripta Mat. 61 (2009) 760. DOI:10.1016/j.scriptamat.2009.06.025
[51] Z. Asghar, G. Requena, H.-P. Degischer, P. Cloetens: Acta Mat. 57 (2009) 4125. DOI:10.1016/j.actamat.2009.05.010
[52] R. Mokso, P. Cloetens, E. Maire, W. Ludwig, J-Y. Buffière: Appl. Phys. Lett. 90 (2007) 144104. DOI:10.1063/1.2719653
[53] A. Pyzalla, B. Camin, T. Buslaps, M. Di Michiel, H. Kaminski, A. Kottar, A. Pernack, W. Reimers: Science 308 (2005) 92. PMid:15802600; DOI:10.1126/science.1106778
[54] M. Di Michiel, J.M. Merino, D. Fernandez-Carreiras, T. Buslaps, V. Honkimäki, P. Falus: Rev. Sci. Instrum. 76 (2005) 043702. DOI:10.1063/1.1884194
[55] S. Terzi, E. Boller, L. Salvo, M. Suéry: International Journal of Cast Metals Research, 22 (2009) 275–278. DOI:10.1179/136404609X368028
[56] O. Lame, D. Bellet, M. Di Michiel, D. Bouvard: Nucl. Instr. Meth. Phys. B 200 (2003) 287–294. DOI:10.1016/S0168-583X(02)01690-7
[57] E. Maire, V. Carmona, J. Courbon, W. Ludwig, Acta Materialia, 6806–6815 (2007). DOI:10.1016/j.actamat.2007.08.043
[58] J. Lambert, I. Cantat, R. Delannay, R. Mokso, P. Cloetens, J.A. Glazier, F. Graner: Phys. Rev. Lett. 99 (2007) 058304. PMid:17930803; DOI:10.1103/PhysRevLett.99.058304
[59] http://www.esrf.eu/UsersAndScience/Experiments/StructMaterials/ID15/
[60] A. Vagnon, O. Lame, D. Bouvard, M. Di Michiel, D. Bellet, G. Kapelski: Acta Mater 54 (2006) 513. DOI:10.1016/j.actamat.2005.09.030
[61] S. Terzi, L. Salvo, M. Suery, A.K. Dahle, E. Boller: Acta Mater 58 (2010) 20. DOI:10.1016/j.actamat.2009.08.052
[62] D. Dzieciol, A. Isaac, F. Sket, A. Borbély, A.R. Pyzalla: Proc. EPD Congress 2009, Characterization of Minerals, Metals and Materials, San Francisco, 14–19 Feb. (2009) 15.
[63] A. Isaac, K. Dzieciol, F. Sket, A. Borbély, A.R. Pyzalla: J. Mechanics and Phys. of Solids (2010) submitted.
[64] B. Budiansky, J.W. Hutchinson, S. Slutsky, in: H.G. Hopkins, M.J. Sewell (Eds.), Mechanics of Solids, Pergamon Press, Oxford (1982) 13.
[65] H. Riedel: Fracture at High Temperatures, Springer Berlin (1987).
[66] N. Kardjilov, I. Manke, M. Strobl, A. Hilger, W. Treimer, M. Meissner, T. Krist, J. Banhart: Nat. Phys. 4 (2008) 399. DOI:10.1038/nphys912
[67] M. Dawson, I. Manke, N. Kardjilov, A. Hilger, J. Banhart: New J. Phys., 11 (2009) 043013. DOI:10.1088/1367-2630/11/4/043013
[68] I. Manke, N. Kardjilov, M. Strobl, A. Hilger, J. Banhart: J. Appl. Phys., 104 (2008) 076109. DOI:10.1063/1.2992516
[69] B.E. Allman, P.J. McMahon, K.A. Nugent, D. Paganin, D.L. Jacobson, M. Arif, S.A. Werner: Nature, 408 (2000) 158. PMid:11089960; DOI:10.1038/35041626
[70] P.J. McMahon, B.E. Allman, K.A. Nugent, D.L. Jacobson, M. Arif, S.A. Werner: Appl. Phys. Lett. 78 (2001) 1011. DOI:10.1063/1.1347387
[71] P.J. McMahon, B.E. Allman, D.L. Jacobson, M. Arif, S.A. Werner, K.A. Nugent: Phys. Rev. Lett. 91 (2003) 145502. PMid:14611534; DOI:10.1103/PhysRevLett.91.145502
[72] S. Zabler: PhD thesis, "X-ray imaging by partially coherent synchrotron light, applied to metallic alloys, tooth dentin and natural rock" (2007).
[73] D. Paganin, S.C. Mayo, T.E. Gureyev, P.R. Miller, S.W. Wolkins: J. Microscopy, 206 (2002) 33. PMid:12000561; DOI:10.1046/j.1365-2818.2002.01010.x
[74] A. Borbély, F.F. Csikor, S. Zabler, P. Cloetens, H. Biermann: Mater. Sci. Eng. A 367 (2004) 40. DOI:10.1016/j.msea.2003.09.068
[75] A. Borbély, P. Kenesei, H. Biermann: Acta Mater. 54 (2006) 2735. DOI:10.1016/j.actamat.2006.02.012

[76] U. Bonse, M.Z. Hart: Physics 189 (1966) 151. DOI:10.1007/BF01327152
[77] D. Chapman, W. Thomlinson, R.E. Johnston, D. Washburn, E. Pisano, N. Gmür, Z. Zhong, R. Menk, F. Arfelli, D. Sayers: Phys. Med. Biol. 42 (1997) 2015. PMid:9394394; DOI:10.1088/0031-9155/42/11/001
[78] F.A. Dilmanian, Z. Zhong, B. Ren, X.Y. Wu, L.D. Chapman, I. Orion, W.C. Thomlinson: Physics in Medicineand Biology, 45 (2000) 933.
[79] W. Treimer, M. Strobl, A. Hilger, C. Seifert, U. Feye-Treimer: Appl. Phys. Lett. 83 (2003) 398. DOI:10.1063/1.1591066
[80] S. Fiedler, A. Bravin, J. Keyrilainen, M. Fernandez, P. Suortti, W. Thomlinson, M. Tenhunen, P. Virkkunen, M.L. Karjalainen-Lindsberg: Physics in Medicine and Biology, 49 (2004) 175. PMid:15083665; DOI:10.1088/0031-9155/49/2/001
[81] M. Strobl, W. Treimer, A. Hilger, NIM B 222 (2004) 653. DOI:10.1016/j.nimb.2004.02.029
[82] P.P. Zhu, J.Y. Wang, Q.X. Yuan, W.X. Huang, H. Shu, B. Gao, T.D. Hu, Z.Y. Wu: Appl. Phys. Lett. 87 (2005) 3.
[83] E. Pagot, S. Fiedler, P. Cloetens, A. Bravin, P. Coan, K. Fezzaa, J. Baruchel, J. Hartwig: Physics in Medicine and Biology 50 (2005) 709. PMid:15773629; DOI:10.1088/0031-9155/50/4/010
[84] M. Strobl, K. Staack, W. Treimer, A. Hilger: Meas. Sci. Technol. 19 (2008) 034020. DOI:10.1088/0957-0233/19/3/034020
[85] T. Weitkamp, A. Diaz, C. David, F. Pfeiffer, M. Stampanoni, P. Cloetens, E. Ziegler: Optics Express 13 (2005) 6296. PMid:19498642; DOI:10.1364/OPEX.13.006296
[86] F. Pfeiffer, T. Weitkamp, O. Bunk, C. David: Nat. Phys. 2 (2006) 258. DOI:10.1038/nphys265
[87] F. Pfeiffer, C. Grünzweig, O. Bunk, G. Frei, E. Lehmann, C. David: Phys. Rev. Lett. 96 (2006) 215505. PMid:16803249; DOI:10.1103/PhysRevLett.96.215505
[88] E. Pagot, P. Cloetens, S. Fiedler, A. Bravin, P. Coan, J. Baruchel, J. Härtwig, W. Thomlinson: Appl. Phys. Lett. 82 (2003) 3421. DOI:10.1063/1.1575508
[89] L. Rigon, H.-J. Besch, F. Arfelli, R.-H. Menk, G. Heitner, H. Plothow-Besch: 3 J. Phys. D: Appl. Phys. 36 (2003) A107.
[90] M. Strobl, W. Treimer, A. Hilger: Appl. Phys. Lett. 85 (2004) 488. DOI:10.1063/1.1774253
[91] F. Pfeiffer, M. Bech, O. Bunk, P. Kraft, E. Eikenberry, C. Brönnimann, C. Grünzweig, C. David: Nat. Mater. 7 (2008) 134. PMid:18204454; DOI:10.1038/nmat2096
[92] M. Strobl, C. Grünzweig, A. Hilger, I. Manke, N. Kardjilov, C. David, F. Pfeiffer: Phys. Rev. Lett. 101 (2008) 123902. PMid:18851372; DOI:10.1103/PhysRevLett.101.123902
[93] M. Strobl, W. Treimer, A. Hilger: Physica B Physica B 385–386 (2006) 1209–1212. DOI:10.1016/j.physb.2006.05.423
[94] K.M. Podurets, V.A. Somenkov, R.R. Chistyakov, S.Sh. Shilstein: Physica B 156–157 (1989) 694–697. DOI:10.1016/0921-4526(89)90766-7
[95] K.M. Podurets, R.R. Chistyakov, S.Sh. Shilshtein: Zh. Tekh. Fiz. 67 (1997)134–136.
[96] M. Strobl, W. Treimer, S. Keil, P. Walter, I. Manke, Appl. Phys. Let. 91 (2007) 254104. DOI:10.1063/1.2825276
[97] C. Grünzweig C. David, O. Bunk, M. Dierolf, G. Frei, G. Kühne, R. Schäfer, S. Pofahl, H.M.R. Rønnow, F. Pfeiffer: Appl. Phys. Lett. 93 (11) (2008) 112504.
[98] N. Kardijlov, A. Hilger, M. Dawson, I. Manke, J. Banhart, M. Strobl, P. Böni: J. Appl. Phys. (in press, 2010).

(Received March 23, 2010; accepted June 28, 2010)

**Bibliography**

DOI 10.3139/146.110382
Int. J. Mat. Res. (formerly Z. Metallkd.)
101 (2010) 9; page 1069–1079

ISSN 1862-5282

**Correspondence address**

Prof. Dr.-Ing. Anke Rita Kaysser-Pyzalla
Helmholtz-Zentrum Berlin für Materialien und Energie GmbH
Hahn-Meitner-Platz 1
14109 Berlin, Germany
Tel.: +49 30 8062 43812
Fax: +49 30 8062 42047
E-mail: anke.pyzalla@helmholtz-berlin.de

You will find the article and additional material by entering the document number **MK110382** on our website at *www.ijmr.de*